ACS APPLIED MATERIALS & INTERFACES

Research Article

www.acsami.org

Three-Dimensional Graphene-Carbon Nanotube Hybrid for High-Performance Enzymatic Biofuel Cells

Kenath Priyanka Prasad,[‡] Yun Chen,[‡] and Peng Chen*

Division of Bioengineering, School of Chemical and Biomedical Engineering, Nanyang Technological University, 70 Nanyang Drive, Singapore 637457, Singapore

Supporting Information

ABSTRACT: Enzymatic biofuel cells (EBFCs) are promising renewable and implantable power sources. However, their power output is often limited by inefficient electron transfer between the enzyme molecules and the electrodes, hindered mass transport, low conductivity, and small active surface area of the electrodes. To tackle these issues, we herein demonstrated a novel EBFC equipped with enzyme-functionalized 3D graphene-single walled carbon nanotubes (SWCNTs) hybrid electrodes using the naturally abundant glucose as the fuel and oxygen as the oxidizer. Such EBFCs, with high stability, can nearly attain the theoretical limit of open circuit voltage (~1.2 V) and a high power density ever reported (2.27 ± 0.11 mW cm^{-2}).

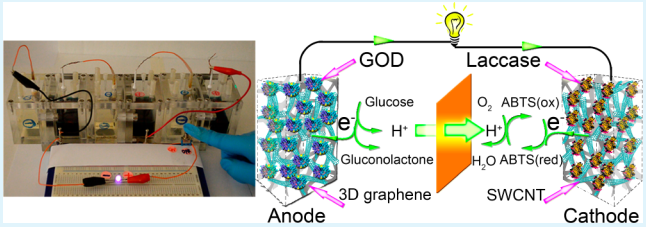

KEYWORDS: *3D graphene, carbon nanotube, enzymatic biofuel cell, green energy, nanomaterials*

INTRODUCTION

Enzymatic biofuel cells (EBFCs) are green energy devices which are capable of harvesting electricity from renewable and abundantly available biofuels using enzymes as the catalysts for oxidation of biofuels (most commonly, glucose) and reduction of oxidizers (most commonly, oxygen).[1−3] As glucose is a ubiquitous fuel in living systems, EBFCs are promising as biocompatible and everlasting power sources for implantable devices.[4−8] The performance (open circuit voltage and power output density) of current EBFCs, however, is often limited by inefficient electron transfer between the enzymes and the electrodes, limited surface area and low conductivity of the electrode, or hindered mass transport.

Because the active centers of the redox enzymes are usually buried inside the protein matrices, the poor electron transfer to the electrode is the primary rate-limiting step for EBFC performance. Carbon nanotubes (CNTs) have therefore been utilized as the conducting nanowires to facilitate electron transfer from the catalytic centers of enzymes to electrode taking advantages of their high electrical conductivity, electrochemical stability, and molecular dimension that enables intimate interaction with the enzymes.[3,9−11] Graphene, the flat cousin of CNTs, has recently attracted enormous interest as electrode material because of its exceptionally high conductivity and specific surface area.[12] More recently, it has been demonstrated that the three-dimensional (3D) architectures of this 2D material can serve as novel 3D electrochemical electrodes for various applications[13] (e.g., energy storage[14] and conversion,[15−17] biological and chemical sensing[18,19]).

Efforts have also been made to achieve synergistic integration of 3D graphene and CNT for applicatons, such as, electrochmeical biosensor,[20] field-emitter devices, and double-layer capacitors.[21] In this study, single-walled CNTs (SWCNTs) decorated 3D graphene was used as both anode and cathode in EBFCs (Figure 1). We demonstrate that EBFCs equipped with enzyme-functionalized 3D graphene-SWCNT hybrid electrodes exhibited greatly improved performance comparing with the previously reported devices, specifically, with an open circuit voltage (E_{cell}^{ocv}) nearly reaching the theoretical limit (~1.2 V), a high power output density (2.27 ± 0.11 mW cm^{-2} or 45.38 ± 2.1 mW cm^{-3}), and good long-term stability (only ~20% drop of E_{cell}^{ocv} after 30 days).

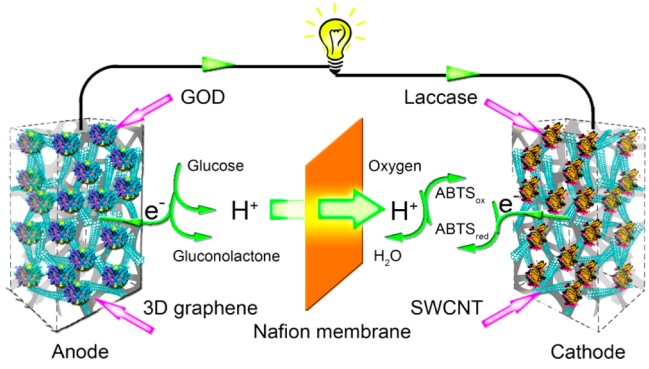

Figure 1. Illustration of the EBFC equipped with 3D graphene-SWCNT hybrid electrodes (not to scale).

Received: November 28, 2013
Accepted: February 17, 2014
Published: February 17, 2014

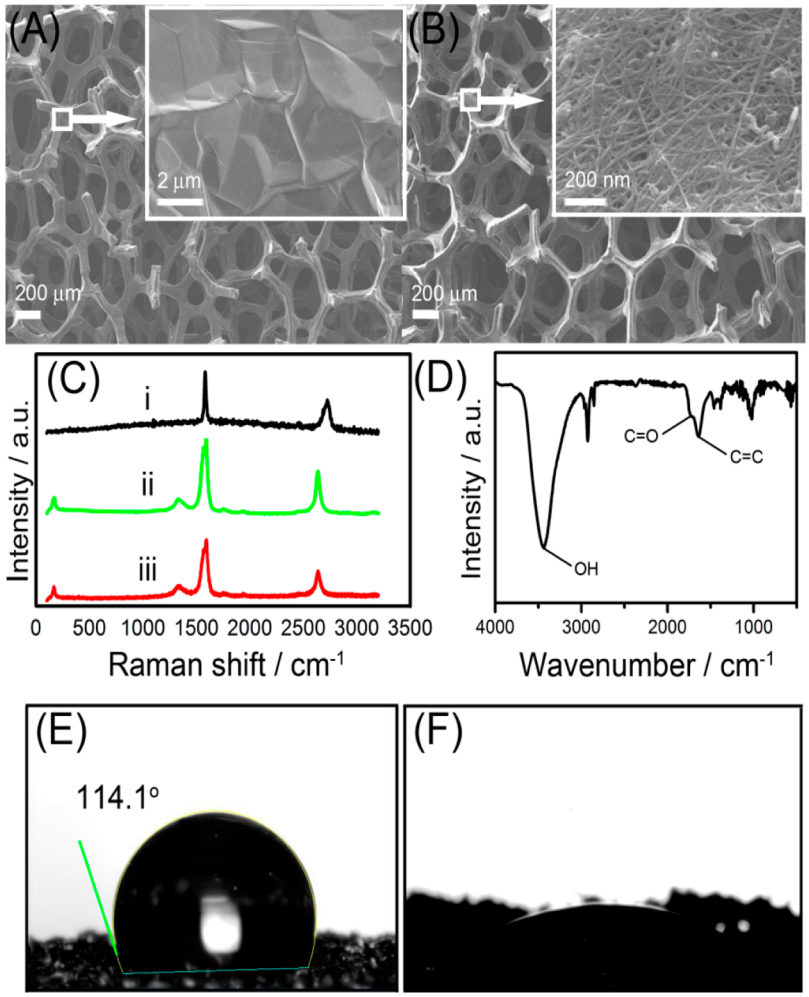

Figure 2. FESEM images of (A) bare 3D graphene and (B) 3D graphene-SWCNT hybrid. Each inset shows the surface of the skeleton at a large magnification. (C) Raman spectra of (i) 3D graphene, (ii) SWCNT and (iii) 3D graphene-SWCNT hybrid. (D) FTIR of SWCNT. Contact angle of (E) 3D graphene and (F) 3D graphene-SWCNT hybrid.

EXPERIMENTAL SECTION

Materials. The nickel (Ni) foams were purchased from Alantum Advanced Technology Materials (China). P3-SWCNT was purchased from Carbon Solutions. Glucose oxidase (GOD, Type VII from *Aspergillus niger*) solution was prepared by dissolving the powder (5 mg mL^{-1}) in a Tris-HCl buffer (pH 8.9, 0.05 M). Laccase (from *Trametes versicolor*) solution was prepared by dissolving the powder in a PBS buffer (pH 7.0, 0.05 M). The electrolyte buffer solution (pH 5.0, 0.2 M) was prepared by sodium acetate and acetic acid.

Characterizations and Measurements. The samples were examined by field emission scanning electron microscopy (FESEM, JMS-6700F), Raman spectroscopy (WITec CRM200 using 633 nm laser), and Fourier transform infrared spectroscopy (Perkin Elmer FTIR Spectrum GX 69233). Cyclic voltammetry (CV) measurements were conducted with an electrochemical workstation (CHI 660D), using a standard three-electrode configuration consisting of a platinum counter electrode, a saturated calomel reference electrode (SCE), and a fabricated 3D working electrode. Open circuit potential was measured between the SCE and the working electrode.

Preparation of 3D Electrodes. 3D graphene was grown using nickel form as the substrate and ethanol as the carbon source using the CVD method, as previously reported.[22] Subsequently, the nickel foam was etched away overnight in 3 M HCl at 60 °C to obtain freestanding 3D graphene foam. To fabricate the electrode, 3D graphene (0.5 cm^2) with the weight of 1.03 mg cm^{-2} was mounted onto a glass slide, and a copper wire fixed and insulated at one end of graphene substrate was used as the electrical lead (Figure S1 in the Supporting Information). Subsequently, the electrode was soaked in P3-SWCNT dispersion (1 mg mL^{-1} in *N*,*N*-dimethylformide) for overnight. After drying at 50 °C for 3 h, an increase in weight of graphene foam was observed (1.45 mg cm^{-2}), indicating the successful deposition of SWCNTs on 3D graphene. The electrode was then dipped into 4 mg mL^{-1} 1-ethyl-3-(3-dimethyl-aminopropyl) carbodiimide hydrochloride (EDC) and *N*-hydroxysuccinimide (NHS) solution for 1 h, followed by conjugation reaction by dipping into the enzyme solutions (GOD or laccase) for 24 h.

Biofuel Cell Design and Test. The EBFC was fabricated in-house using acrylic glass. The perfluorosulfonic acid/PTFE copolymer membrane (25.4 μm thick, Nafion) that separates the anodic and cathodic chambers was purchased from DuPont (Figure S1 in the Supporting Information). In anodic chamber, the buffer electrolyte solution (pH 5.0, 0.2 M) made of sodium acetate and acetic acid was saturated with nitrogen and contained a defined amount of glucose. Cathodic chamber containing the same buffer solution was saturated with oxygen and contained 0.5 mM 2,2′-azinobis (3-ethylbenzothiazoline-6-sulfonic acid) diammonium salt (ABTS).

The E_{cell}^{ocv} of the EBFC was measured using CHI-660D electrochemical station. At steady state E_{cell}^{ocv}, the EBFC was loaded with an external resistance varying from 100 Ω ~ 100 kΩ to determine the polarization and power output density. The operation of the EBFC was at room temperature (25 ± 1 ∘C)

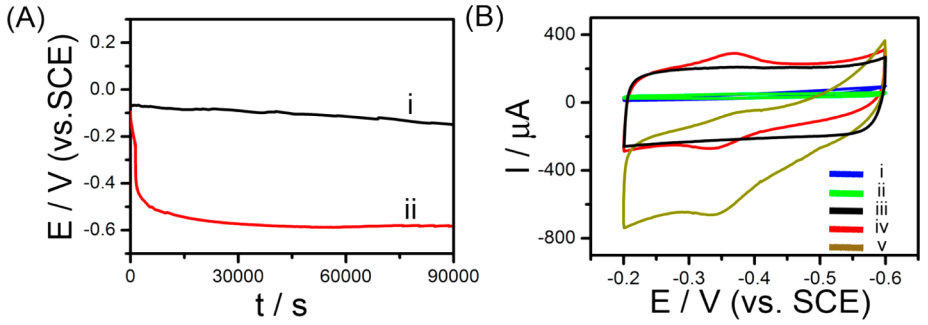

Figure 3. (A) The open circuit potential of (i) the 3D graphene-GOD anode and (ii) 3D graphene-SWCNT-GOD anode in pH 5.0 electrolyte solution containing 30 mM glucose. (B) The CVs of (i) 3D graphene electrode, (ii) 3D graphene-GOD electrode, (iii) 3D graphene-SWCNT hybrid electrode, and (iv) 3D graphene-SWCNT-GOD hybrid electrode in pH 5.0 electrolyte solution. (v) 3D graphene-SWCNT-GOD hybrid electrode in pH 5.0 electrolyte solution containing 1 mM glucose.

RESULTS AND DISCUSSION

Material Characterizations. 3D graphene, synthesized by chemical vapor deposition using nickel foam as the growth substrate, is a monolithic macroporous structure as revealed by scanning electron microscopy (Figure 2A). SWCNTs can be adsorbed onto 3D graphene scaffold simply by incubation with SWCNT dispersion in N,N-dimethylmethanamide (DMF). As shown Figure 2B, 3D graphene is covered inside-out by a dense thin-film network of SWCNTs with a mesh size comparable to a macromolecule. Bare 3D graphene is mainly few-layered (as indicated by the ratio between 2D and G band) and defect-free (as indicated by the absence of D band).[23] The 3D graphene-SWCNT hybrid exhibits characteristic D band from SWCNTs. The used SWCNTs are carboxylated. This is confirmed by Fourier transform infrared spectroscopy (FTIR) (Figure 2D). The amphiphilic carboxylated SWCNTs, on the one hand, firmly interact with graphene through pi-pi and hydrophobic interaction;[24−26] on the other hand, make the hybrid structure hydrophilic as evidenced by the contact angel measurement (Figure 2E and F) which is important to ensure electrolyte penetration. Furthermore, SWCNT coating can further increase the surface area of the electrode. Finally, the hybrid electrode was covalently functionalized with GOD for anode or with laccase for cathode *via* covalent bonding between the carboxyl group on SWCNT and amino group on the protein.

The Anodic Properties. As demonstrated in Figure 3A, the anodic open circuit potential (E_a^{ocp}) of the 3D graphene-SWCNT-GOD hybrid electrode in the presence of 30 mM glucose is ∼−0.58 V (±0.01, n = 3 electrodes) which is close to the theoretical limit determined by the thermodynamic equilibrium of the gluconolactone/glucose couple (−0.57 V).[27,28] This is significantly higher than the previously reported values.[29] In contrast, E_a^{ocp} of GOD coated bare 3D graphene is only ∼−0.12 V (±0.005, n = 3), suggesting the critical role of SWCNTs. Cyclic voltammetry (CV) of GOD functionalized hybrid electrode shows a pair of prominent redox peaks (at −0.337 V and −0.363 V, respectively) in perfect accordance with the oxidation and reduction potentials of the redox active center (flavin adenine dinucleotide, FAD) of GOD (Figure 3B).[30] This observation unambiguously indicates the successful immobilization of GODs on the electrode surface and good electrical coupling (direct electron transfer - DET)[31,32] between the enzymes and the electrode. To further support this, it is observed that addition of glucose leads to obvious increase of the oxidative current and dramatic decrease of the reductive current in CV. In the absence of O_2, the observed CV is resulting from the direct electrochemistry of the active center of GOD as follows:[33,34]

$$\text{GOD (FAD)} + \text{glucose} \rightarrow \text{GOD (FADH}_2\text{)} + \text{gluconolactone} \quad (1)$$

$$\text{GOD (FADH}_2\text{)} \rightarrow \text{GOD (FAD)} + 2\text{H}^+ + 2\text{e}^- \quad (2)$$

In addition, the onset oxidation potential in the presence of glucose is about −0.550 V, which is consistent with the E_a^{ocp} of the 3D graphene-SWCNT-GOD anode in the glucose solution.[35−37] The uniform coating of a nonconductive layer of proteins is confirmed by FESEM image, in which the SWCNT mesh becomes blurry due to snugly trapping of proteins (Figure S2 in the Supporting Information). As expected, these redox peaks are absent in the GOD-free hybrid electrode. In comparison, we demonstrated that both of the 3D graphene and 3D graphene-SWCNT hybrid exhibit no catalytic activities to glucose (Figure S3A). The bare 3D graphene electrode coated with GODs *via* physioadsorption demonstrates weak redox peaks of GODs and weak response towards glucose (Figure S3B), presumably due to low abundance of GODs, possible denaturing of GOD on the flat graphene surface, and poor interaction between the enzymes and the electrode. In support of this, FESEM reveals that GODs only sparsely adhere onto the smooth graphene surface as clusters preferably on the wrinkles (Figure S2 in the Supporting Information).

In order to evaluate the electron transfer, the CVs of the 3D graphene-SWCNT-GOD electrode were investigated at different scan rates. As shown in Figure S4 (Supporting Information), the formal potential ($E^{0'}$ − the average between the reduction and oxidation potentials) of GOD remains unchanged with increasing scan rates, and both the anodic and cathodic peak currents (their ratio is close to 1) proportionally increase with scan rates. These observations suggest that the redox of GOD is a reversible and surface-confined process. According to the following equation, $i_p = nFQv/4RT$ (where i_p = redox peak current; Q = integrated charge of the redox peak; v = scan rate; F = Faraday constant; R = gas constant; T = temperature),[38] the number of charges transferred from GOD redox reaction (n) is calculated to be 2 which is the theoretical value of FAD to $FADH_2$ conversion in the active center of GOD. This indicates the excellent electrical coupling between GOD and electrode. Furthermore, the small peak−peak separation (the different between the oxidative and reductive peaks, ∼29 mV) also nicely agrees with the theoretical value

dx.doi.org/10.1021/am405432b | ACS Appl. Mater. Interfaces 2014, 6, 3387−3393

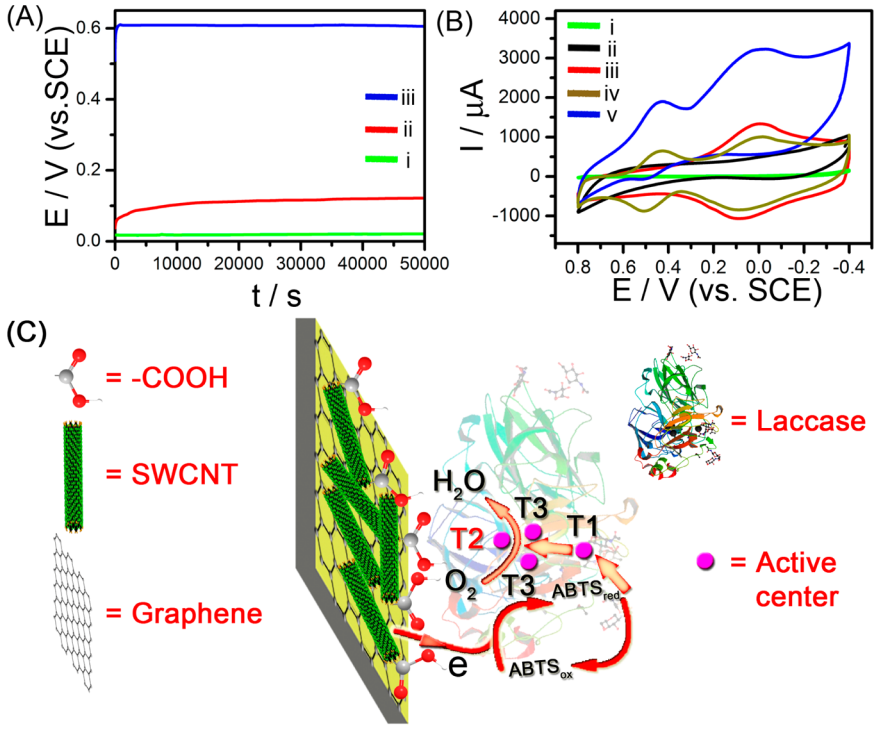

Figure 4. (A) The open circuit potential (measured in pH 5.0 electrolyte solution saturated with O_2) of (i) 3D graphene-laccase cathode and (ii) 3D graphene-SWCNT-laccase cathode, and (iii) 3D graphene-SWCNT-laccase cathode (with 0.5 mM ABTS). (B) The CVs of (i) 3D graphene-laccase electrode (solution with saturated N_2), (ii) 3D graphene-SWCNT hybrid electrode (solution with saturated N_2), (iii) 3D graphene-SWCNT-laccase hybrid electrode (solution with saturated N_2), (iv) 3D graphene-SWCNT-laccase hybrid electrode (solution saturated with N_2 and containing 0.5 mM ABTS), and (v) 3D graphene-SWCNT-laccase hybrid electrode (solution saturated with O_2 and containing 0.5 mM ABTS). (C) Illustration of electron transfer pathways.

($\ln 10 * R * T/F/n$), indicating the electron transfer kinetics is fast enough to maintain the Nernst equilibrium of GOD's redox transition. Based on Laviron's theory,[39] $k_s = mnFv/RT$ (where m is a constant determined by the separation between oxidative and reductive peaks),[40] the electron transfer rate constant k_s can be calculated to be 12.52 ± 0.84 s^{-1}, which is much higher than the previously reported values obtained from graphene (2.83 s^{-1}),[41] multiwalled carbon nanotubes (1.53 s^{-1}),[42] boron-doped carbon nanotubes (1.56 s^{-1}),[43] or single-walled carbon nanohorns (3.0 s^{-1})[44] based electrodes.

In the ideal situation (reversible and unhindered electrical coupling between a monolayer of electroactive enzyme and the underlying electrode), the CV is predicted to have symmetric redox peaks with zero gap between the oxidation and reduction potentials and a peak-width at half height of 90.6 mV/n (here, n = 2).[45] These are indeed observed at a slow scan rate of 1 mV s^{-1} (Figure S5 in the Supporting Information), indicating that the electron transfer between GOD and electrode is ideally reversible at such a rate. Furthermore, we demonstrate that E^0, decreases linearly with the increase of pH with a slope nearly equal to the theoretical value of 58.6 mV/pH (Figure S6 in the Supporting Information), suggesting a reversible electrochemical process with equal-number (n = 2) of electrons and protons involved the GOD redox reaction: GOD ($FADH_2$) ↔ GOD (FAD) + $2e^-$ + $2H^+$.[46,47]

The Cathodic Properties. As demonstrated in Figure 4A, the cathodic open circuit potential (E_c^{ocp}) of the laccase coated 3D graphene electrode (with saturated oxygen, at pH 5.0) is close to 0 V (0.02 ± 0.0003 V, n = 3), essentially due to poor adhesion of laccase proteins on graphene surface (Figure S2 in the Supporting Information). In comparison, E_c^{ocp} reaches ~0.11 V (±0.002, n = 3) when using 3D graphene-SWCNT-laccase electrode. Despite that SWCNTs assist to abundantly and snugly anchor the enzymes, the obtained E_c^{ocp} is still far from the theoretical limit (0.61 V)[27,28] suggesting that the electron transfer from the active centers of laccase to electrode is hindered. ABTS is an electron transfer mediator often used to facilitate the electron transfer from laccase. As shown (Figure 4A), in the presence of ABTS (0.5 mM), E_c^{ocp} of the 3D graphene-SWCNT-laccase electrode is boosted nearly to the theoretical thermodynamic equilibrium of the O_2/H_2O couple (0.6 ± 0.01 V, n = 3). These observations suggest that ABTS molecules facilitate the electron transfer from oxygen reduction.

Consistently, it is found that the CVs of the 3D graphene-laccase electrode or bare 3D graphene-SWCNT electrode are absent of obvious redox peaks from laccase redox transition, whereas a pair of prominent redox peaks (at −0.003 V and 0.086 V, respectively) are observed from the 3D graphene-SWCNT-laccase electrode corresponding to the T2 redox active center of laccase (Figure 4B). This confirms the good coupling between the enzymes and the 3D graphene-SWCNT substrate. The redox of laccase on the electrode is a reversible and surface-confined process, as evidenced by the linear scaling between redox currents and scan rate (Figure S7 in the Supporting Information). In comparison, the bare 3D graphene electrode, 3D graphene-SWCNT hybrid electrode, and laccase functionalized 3D graphene electrode shows little catalytic action to O_2 (Figure S8 in the Supporting Information).

As illustrated in Figure 4C, laccase has multiple catalytic centers (T1-T3). The redox peaks in the CV of the 3D graphene-SWCNT-laccase electrode coincide with the redox potentials of T2 center, suggesting that the T2 center of laccase

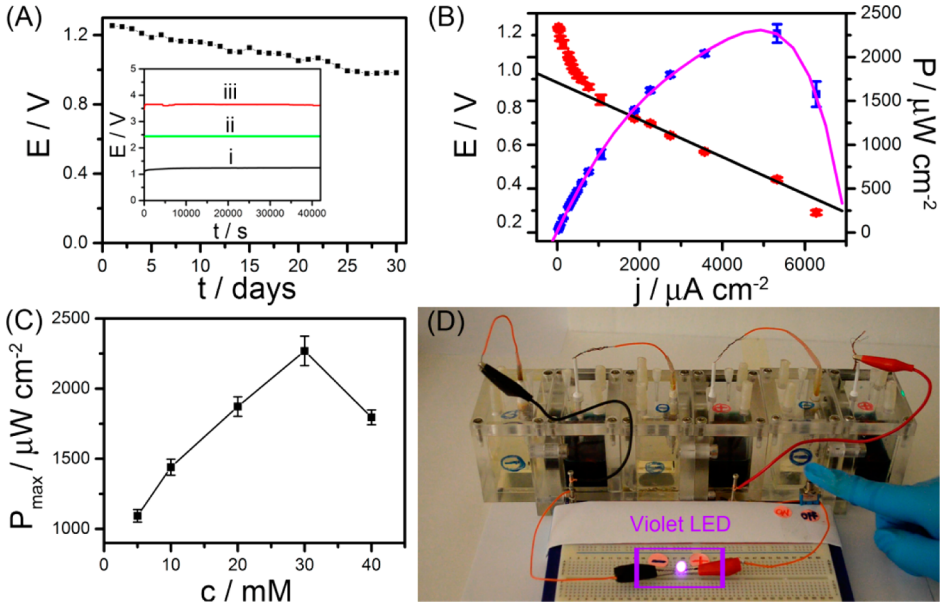

Figure 5. (A) The open circuit voltage from one cell over 30 days. Inset: the open circuit voltages from (i) single EBFC, (ii) double EBFCs, and (iii) triple EBFCs in series. (B) Polarization curve and power output curve of the EBFC. (C) The maximum power output of the EBFC with different glucose concentrations. (D) A violet LED powered by three EBFCs in series.

is in close approximation to the electrode surface to allow direct electron transfer (Figure 4B).[48,49] However, it is known the involvement of the T1 center is crucial to achieve efficient oxygen reduction and thus high open circuit potential.[50] Without the ABTS mediator, the T1 center whose oxidation potential is close to the potential of oxygen reduction is not able to participate in the reaction. Therefore, the electron transfer with sole involvement of T2 center is not efficient due to a large energy barrier between oxidation of T2 center and oxygen reduction. Because the redox potential of ABTS matches well with that of the T1 center,[51,52] the diffusive small ABTS molecules can assist to transfer electrons to the T1 center of laccase that is distant to the electrode surface,[53,54] whereby electrons are intramolecularly passed to the T2/T3 cluster (the oxygen reduction site).[55] Therefore, in the presence of ABTS mediator, E_c^{ocp} approaches the thermodynamic equilibrium of the O_2/H_2O couple due to the good electrical coupling between the electrode and the catalytic centers of laccase. As shown in Figure 4B, the CV of the 3D graphene-SWCNT-laccase electrode exhibits an additional pair of redox peaks at 0.426 V and 0.508 V due to ABTS.[56] In the presence of saturated oxygen, the oxidative peak of ABTS decreases, while its reductive peak increases confirming the participation of ABTS in the oxygen reaction.[51] The onset reduction potential is around 0.60 V, which coincides with the measured E_c^{ocp} of the 3D graphene-SWCNT-laccase cathode.[35−37] Consistently, in the presence of saturated oxygen, the oxidative peak of T2 center in the CV decreases, while its reductive peak increases confirming the involvement of the T2 center in electron transfer from oxygen reduction (Figure 4B).

The Characters of the EBFC. The enzymatic biofuel cells (EBFCs) were fabricated with a 3D graphene-SWCNT-GOD anode and a 3D graphene-SWCNT-laccase cathode as illustrated in Figure 1. As demonstrated in Figure 5, the E_{cell}^{ocv} of the EBFC reaches ~1.20 V, close to the theoretical potential difference between the O_2/H_2O couple and the gluconolactone/glucose couple at thermodynamic equilibrium.[4] To the best of our knowledge, this has not been attained in any of the previous studies. In addition, only a 20% drop of E_{cell}^{ocv} is observed after 30 days, indicating the high stability of our EBFCs. Figure 5B displays the typical polarization curve and power output curve of the EBFC when the glucose concentration in the anolyte was 30 mM. The internal resistance of the EBFC was calculated to be 245 Ω, based on the fitting of the linear region of the polarization curve. The maximal power output (P_{max}) density is 2.27 ± 0.11 mW cm^{-2} (n = 3), which is the highest value ever reported for glucose-based EBFCs. It is superior to the previously reported best performance using a graphene electrode[57] and a carbon nanotube based electrode[29] as well as other carbon electrodes.[58] Figure 5C shows a bell-shaped dependence of P_{max} on glucose concentration with the optimal concentration of ~30 mM. Three EBFCs in the series are able to lighten up a violet LED whose turn-on voltage is ~3 V.

CONCLUSIONS

A novel glucose/O_2 powered EBFC equipped with a 3D graphene-SWCNT-GOD bioanode and a 3D graphene-SWCNT-laccase cathode is developed. Such EBFC is able to approach the theoretical limit of open circuit voltage (1.2 V) and a high power density (2.27 ± 0.11 mW cm^{-2}) due to the following reasons. Firstly, 3D graphene provides a large surface area for abundant loading of enzymes and for catalytic reactions. Secondly, the nanotopographic surface and chemical handles provided by SWCNT networks ensure snug anchoring of enzyme molecules. Thirdly, nearly perfect electrical coupling between the enzymes and the electrodes for efficient direct electron transfer is achieved due to intimate interaction between the enzymes and the electrodes as well as the electron shuttling by ABTS molecules at the cathode. Finally, the 3D multiplexed and continuous conduction networks offered by the 3D graphene-SWCNT substrate ensure rapid charge transfer and conduction. This study demonstrates the synergistic integration between the two carbon isotopes (graphene and carbon nanotubes) and the new performance boundaries of glucose-powered EBFCs.

■ ASSOCIATED CONTENT

Supporting Information

The engineering drawing, the scenograph and optical image of the biofuel cell; FESEM images of 3D graphene-GOD electrode, 3D graphene-SWCNT-GOD electrode, 3D graphene-laccase electrode, and 3D graphene-SWCNT-laccase electrode; CVs of the 3D graphene electrode, 3D graphene-SWCNT electrode, and 3D graphene-GOD electrode to glucose; CVs of the 3D graphene-SWCNT-GOD hybrid electrode at different scan rates; CV of the 3D graphene-SWCNT-GOD electrode at the scan rate of 1 mV s^{-1}; CVs of the 3D graphene-SWCNT-GOD electrode in electrolyte solution with different pH values; CVs of the 3D graphene-SWCNT-laccase hybrid electrode at different scan rates; CVs of the 3D graphene electrode, 3D graphene-SWCNT electrode, and 3D graphene-laccase electrode to O_2. This material is available free of charge via the Internet at http://pubs.acs.org.

■ AUTHOR INFORMATION

Corresponding Author

*E-mail: chenpeng@ntu.edu.sg.

Author Contributions

‡These authors contributed equally. The manuscript was written through contributions of all authors. All authors have given approval to the final version of the manuscript.

Notes

The authors declare no competing financial interest.

■ ACKNOWLEDGMENTS

This work was supported by a SERC Grant (#102 170 0142) from the Agency for Science, Technology and Research (A*STAR, Singapore), an AcRF tier 2 grant (MOE2011-T2-2-010) from Ministry of Eduction (Singapore), and NNSF of China (61328401).

■ REFERENCES

(1) Moehlenbrock, M. J.; Minteer, S. D. *Chem. Soc. Rev.* **2008**, *37*, 1188−1196.
(2) Cooney, M. J.; Svoboda, V.; Lau, C.; Martin, G.; Minteer, S. D. *Energy Environ. Sci.* **2008**, *1*, 320−337.
(3) Yang, X. Y.; Tian, G.; Jiang, N.; Su, B. L. *Energy Environ. Sci.* **2012**, *5*, 5540−5563.
(4) Barton, S. C.; Gallaway, J.; Atanassov, P. *Chem. Rev.* **2004**, *104*, 4867−4886.
(5) Schroder, U. *Angew. Chem., Int. Ed.* **2012**, *51*, 7370−7372.
(6) MacVittie, K.; Halamek, J.; Halamkova, L.; Southcott, M.; Jemison, W. D.; Lobeld, R.; Katz, E. *Energy Environ. Sci.* **2013**, *6*, 81−86.
(7) Zebda, A.; Cosnier, S.; Alcaraz, J. P.; Holzinger, M.; Le Goff, A.; Gondran, C.; Boucher, F.; Giroud, F.; Gorgy, K.; Lamraoui, H.; Cinquin, P. *Sci. Rep.* **2013**, *3*, 1516.
(8) Yoshino, S.; Miyake, T.; Yamada, T.; Hata, K.; Nishizawa, M. *Adv. Energy Mater.* **2013**, *3*, 60−64.
(9) Minteer, S. D.; Atanassov, P.; Luckarift, H. R.; Johnson, G. R. *Mater. Today* **2012**, *15*, 166−173.
(10) Feng, W.; Ji, P. J. *Biotechnol. Adv.* **2011**, *29*, 889−895.
(11) Vashist, S. K.; Zheng, D.; Al-Rubeaan, K.; Luong, J. H. T.; Sheu, F. S. *Biotechnol. Adv.* **2011**, *29*, 169−188.
(12) Zhao, C. E.; Wang, Y.; Shi, F. J.; Zhang, J. R.; Zhu, J. J. *Chem. Commun.* **2013**, *49*, 6668−6670.
(13) Nardecchia, S.; Carriazo, D.; Ferrer, M. L.; Gutierrez, M. C.; del Monte, F. *Chem. Soc. Rev.* **2013**, *42*, 794−830.
(14) Choi, B. G.; Yang, M.; Hong, W. H.; Choi, J. W.; Huh, Y. S. *ACS Nano* **2012**, *6*, 4020−4028.
(15) Chen, W. F.; Li, S. R.; Chen, C. H.; Yan, L. F. *Adv. Mater.* **2011**, *23*, 5679−5683.
(16) Yong, Y. C.; Dong, X. C.; Chan-Park, M. B.; Song, H.; Chen, P. *ACS Nano* **2012**, *6*, 2394−2400.
(17) Maiyalagan, T.; Dong, X. C.; Chen, P.; Wang, X. *J. Mater. Chem.* **2012**, *22*, 5286−5290.
(18) Dong, X. C.; Wang, X. W.; Wang, L. H.; Song, H.; Zhang, H.; Huang, W.; Chen, P. *ACS Appl. Mater. Interfaces* **2012**, *4*, 3129−3133.
(19) Xi, F. N.; Zhao, D. J.; Wang, X. W.; Chen, P. *Electrochem. Commun.* **2013**, *26*, 81−84.
(20) Dong, X. C.; Ma, Y. W.; Zhu, G. Y.; Huang, Y. X.; Wang, J.; Chan-Park, M. B.; Wang, L. H.; Huang, W.; Chen, P. *J. Mater. Chem.* **2012**, *22*, 17044−17048.
(21) Yan, Z.; Ma, L. L.; Zhu, Y.; Lahiri, I.; Hahm, M. G.; Liu, Z.; Yang, S. B.; Xiang, C. S.; Lu, W.; Peng, Z. W.; Sun, Z. Z.; Kittrell, C.; Lou, J.; Choi, W. B.; Ajayan, P. M.; Tour, J. M. *ACS Nano* **2013**, *7*, 58−64.
(22) Dong, X. C.; Cao, Y. F.; Wang, J.; Chan-Park, M. B.; Wang, L. H.; Huang, W.; Chen, P. *RSC Adv.* **2012**, *2*, 4364−4369.
(23) Chen, Z. P.; Ren, W. C.; Gao, L. B.; Liu, B. L.; Pei, S. F.; Cheng, H. M. *Nat. Mater.* **2011**, *10*, 424−428.
(24) Zhao, M. Q.; Liu, X. F.; Zhang, Q.; Tian, G. L.; Huang, J. Q.; Zhu, W. C.; Wei, F. *ACS Nano* **2012**, *6*, 10759−10769.
(25) Lu, L. H.; Liu, J. H.; Hu, Y.; Zhang, Y. W.; Randriamahazaka, H.; Chen, W. *Adv. Mater.* **2012**, *24*, 4317−4321.
(26) Zhang, D. S.; Yan, T. T.; Shi, L. Y.; Peng, Z.; Wen, X. R.; Zhang, J. P. *J. Mater. Chem.* **2012**, *22*, 14696−14704.
(27) Harris, D. C. In *Quantitative chemical analysis*, 8th ed.; W. H. Freeman and Company: New York, 2010; p 298.
(28) Chen, Y.; Prasad, K. P.; Wang, X. W.; Pang, H. C.; Yan, R. Y.; Than, A.; Chan-Park, M. B.; Chen, P. *Phys. Chem. Chem. Phys.* **2013**, *15*, 9170−9176.
(29) Zebda, A.; Gondran, C.; Le Goff, A.; Holzinger, M.; Cinquin, P.; Cosnier, S. *Nat. Commun.* **2011**, *2*, 370.
(30) Shan, C. S.; Yang, H. F.; Song, J. F.; Han, D. X.; Ivaska, A.; Niu, L. *Anal. Chem.* **2009**, *81*, 2378−2382.
(31) Bao, S. J.; Li, C. M.; Zang, J. F.; Cui, X. Q.; Qiao, Y.; Guo, J. *Adv. Funct. Mater.* **2008**, *18*, 591−599.
(32) Guo, C. X.; Hu, F. P.; Lou, X. W.; Li, C. M. *J. Power Sources* **2010**, *195*, 4090−4097.
(33) Goran, J. M.; Mantilla, S. M.; Stevenson, K. J. *Anal. Chem.* **2013**, *85*, 1571−1581.
(34) Wang, Z. Y.; Liu, S. N.; Wu, P.; Cai, C. X. *Anal. Chem.* **2009**, *81*, 1638−1645.
(35) Wen, D.; Xu, X. L.; Dong, S. J. *Energy Environ. Sci.* **2011**, *4*, 1358−1363.
(36) Li, X. C.; Zhou, H. J.; Yu, P.; Su, L.; Ohsaka, T.; Mao, L. Q. *Electrochem. Commun.* **2008**, *10*, 851−854.
(37) Yan, Y. M.; Yehezkeli, O.; Willner, I. *Chem.—Eur. J.* **2007**, *13*, 10168−10175.
(38) Laviron, E. *J. Electroanal. Chem.* **1979**, *100*, 263−270.
(39) Laviron, E. *J. Electroanal. Chem.* **1979**, *101*, 19−28.
(40) Liu, S. Q.; Ju, H. X. *Biosens. Bioelectron.* **2003**, *19*, 177−183.
(41) Kang, X. H.; Wang, J.; Wu, H.; Aksay, I. A.; Liu, J.; Lin, Y. H. *Biosens. Bioelectron.* **2009**, *25*, 901−905.
(42) Cai, C. X.; Chen, J. *Anal. Biochem.* **2004**, *332*, 75−83.
(43) Deng, C. Y.; Chen, J. H.; Chen, X. L.; Mao, C. H.; Nie, L. H.; Yao, S. Z. *Biosens. Bioelectron.* **2008**, *23*, 1272−1277.
(44) Liu, X. Q.; Shi, L. H.; Niu, W. X.; Li, H. J.; Xu, G. B. *Biosens. Bioelectron.* **2008**, *23*, 1887−1890.
(45) Rusling, J. F.; Wang, B.; Yun, S.-e. In *Bioelectrochemistry: Fundamentals, Experimental Techniques and Applications*; Bartlett, P., Eds.; John Wiley & Sons, Ltd.: New York, 2008; Chapter 2, pp 39−85.
(46) Razmi, H.; Mohammad-Rezaei, R. *Biosens. Bioelectron.* **2013**, *41*, 498−504.
(47) Yang, Z.; Ren, Y.; Zhang, Y.; Li, J.; Li, H.; Hu, X. H.; Xu, Q. *Biosens. Bioelectron.* **2011**, *26*, 4337−4341.
(48) Frasconi, M.; Boer, H.; Koivula, A.; Mazzei, F. *Electrochim. Acta* **2010**, *56*, 817−827.

(49) Ivnitski, D. M.; Khripin, C.; Luckarift, H. R.; Johnson, G. R.; Atanassov, P. *Electrochim. Acta* **2010**, *55*, 7385−7393.
(50) Klis, M.; Karbarz, M.; Stojek, Z.; Rogalski, J.; Bilewicz, R. *J. Phys. Chem. B* **2009**, *113*, 6062−6067.
(51) Liu, Y.; Wang, M. K.; Zhao, F.; Liu, B. F.; Dong, S. J. *Chem.—Eur. J* **2005**, *11*, 4970−4974.
(52) Liu, Y.; Dong, S. J. *Electrochem. Commun.* **2007**, *9*, 1423−1427.
(53) Szamocki, R.; Flexer, V.; Levin, L.; Forchiasin, F.; Calvo, E. J. *Electrochim. Acta* **2009**, *54*, 1970−1977.
(54) Pita, M.; Gutierrez-Sanchez, C.; Olea, D.; Velez, M.; Garcia-Diego, C.; Shleev, S.; Fernandez, V. M.; De Lacey, A. L. *J. Phys. Chem. C* **2011**, *115*, 13420−13428.
(55) Lau, C.; Adkins, E. R.; Ramasamy, R. P.; Luckarift, H. R.; Johnson, G. R.; Atanassov, P. *Adv. Energy Mater.* **2012**, *2*, 162−168.
(56) Brunel, L.; Denele, J.; Servat, K.; Kokoh, K. B.; Jolivalt, C.; Innocent, C.; Cretin, M.; Rolland, M.; Tingry, S. *Electrochem. Commun.* **2007**, *9*, 331−336.
(57) Liu, C.; Alwarappan, S.; Chen, Z. F.; Kong, X. X.; Li, C. Z. *Biosens. Bioelectron.* **2010**, *25*, 1829−1833.
(58) Sakai, H.; Nakagawa, T.; Tokita, Y.; Hatazawa, T.; Ikeda, T.; Tsujimura, S.; Kano, K. *Energy Environ. Sci.* **2009**, *2*, 133−138.